

## A SURVEY FOR FAST TRANSIENTS IN THE FORNAX CLUSTER OF GALAXIES

A. RAU<sup>1</sup>, E.O. OFEK<sup>1</sup>, S.R. KULKARNI<sup>1</sup>, B.F. MADORE<sup>2</sup>, O. PEVUNOVA<sup>3</sup>, M. AJELLO<sup>4</sup>

*Accepted for Publication in Astrophysical Journal*

### ABSTRACT

The luminosity gap between novae ( $M_R \leq -10$ ) and supernovae ( $M_R \geq -14$ ) is well known since the pioneering research of Zwicky and Hubble. Nearby galaxy clusters and concentrations offer an excellent opportunity to search for explosions brighter than classical novae and fainter than supernovae. Here, we present the results of a *B*-band survey of 23 member galaxies of the Fornax cluster, performed at the Las Campanas 2.5-m Irene duPont telescope. Observations with a cadence of 32 minutes discovered no genuine fast transient to a limiting absolute magnitude of  $M_B = -9.3$  mag. We provide a detailed assessment of the transient detection efficiency and the resulting upper limits on the event rate as function of peak magnitude. Further, we discuss the discoveries of five previously unknown foreground variables which we identified as two flare stars, two W Uma type eclipsing binaries and a candidate  $\delta$  Scuti/SX Phe star.

*Subject headings:* surveys — stars: flare — (stars: variables:) delta Scuti — stars: variables: other

### 1. INTRODUCTION

The recent findings of a number of enigmatic transients, e.g., new types of novae (Kulkarni et al. 2007) and supernovae related events (Ofek et al. 2007a; Smith et al 2007; Quimby et al. 2007; Pastorello et al. 2007), have demonstrated that the phase space of eruptive transients is already richer than discussed in astronomy texts. Even more discoveries, especially on timescales of days to weeks, are anticipated for the upcoming large-area facilities, such as SkyMapper (Schmidt et al. 2005), the Panoramic Survey Telescope and Rapid Response System (Pan-STARRS; Kaiser et al. 2002), and the Large Synoptic Survey Telescope (LSST; Tyson 2005). However, on shorter timescales (minutes to hours), their observational designs are less optimal and dedicating, small experiments are more likely to lead to great findings. A small number of such surveys have been performed previously (e.g., Becker et al. 2004; Rykoff et al. 2005; Morales-Rueda et al. 2006; Ramsay et al. 2006) and informed us of the difficulty of discovering genuine new classes of fast transients and variables<sup>5</sup>. Here, the greatest challenge is to pierce the fog of known foreground contaminants. Asteroids and flares from M dwarfs have been established to dominate the short-timescale variable sky (Kulkarni & Rau 2006). However, once this curtain is penetrated, exciting and rare events can be found, e.g., the high-amplitude optical flickering ( $\sim 3.5$  mag in 6 min) accompanying the outburst of

the Galactic X-ray binary Swift J195509.6+261406 (Stefanescu et al. 2007; Kasliwal et al. 2007). The latter source was brought to attention by its preceding gamma-ray flare (Pagani et al. 2007). Nonetheless, high-cadence optical surveys will be capable of detecting similar events independently of the high-energy emission.

Another, yet unidentified, bright ( $R = 11.7$  mag), high-amplitude candidate transient ( $>6$  mag in 2 min) was recently discovered along the line of sight to the nearby ( $\sim 70$  Mpc) galaxy IC 4779 (Klotz et al. 2007). If associated with IC 4779, the event reached a staggering peak luminosity of  $L_{R,\text{peak}} \sim 3 \times 10^{44}$  erg s<sup>-1</sup>, outshined only by the brightest known supernova (SN2005ap; Quimby et al. 2007).

A critical component of every successful transient search is a judicious target selection. This is especially relevant for short-cadence experiment, where only a small number of fields is repeatedly observed. Obvious targets for such a search are nearby massive clusters of galaxies. Clusters contain a large stellar mass, which increases the probability of finding rare events during the transient phase. Furthermore, their known distance provides a direct access to the absolute brightness of the events. In addition, the variety of galaxy types, and thus stellar populations, may offer constraints on the progenitor ages.

In this paper we present the results of an optical survey of galaxies in the Fornax Cluster designed to test the transient and variable sky in a galaxy cluster environment on timescales shorter than one hour. At the distance of  $16.2 \pm 1.5$  Mpc ( $(m - M)_0 = 30.91 \pm 0.19$ ; Grillmair et al. 1999) and with negligible foreground extinction ( $E(B-V) = 0.013$  mag; Schlegel et al. 1998) observations of the Fornax cluster allow one to probe the gap in absolute peak brightness between classical novae ( $M_R > -10$ ) and supernovae ( $M_R < -14$ ) already with 2-m-class telescopes. This part of phase space has become particularly alluring with the recognition of an emerging population of new types of explosions, namely the Luminous Red Novae (Kulkarni et al. 2007; Rau et al. 2007; Ofek et al. 2007b).

Electronic address: arne@astro.caltech.edu

<sup>1</sup> Caltech Optical Observatories, MS 105-24, California Institute of Technology, Pasadena, CA 91125, USA

<sup>2</sup> Observatories of the Carnegie Institution of Washington, 813 Santa Barbara Street, Pasadena, CA 91101, USA

<sup>3</sup> Infrared Processing and Analysis Center, MS 100-22, California Institute of Technology, Jet Propulsion Laboratory, Pasadena, CA 91125, USA

<sup>4</sup> Max-Planck Institut für Extraterrestrische Physik, Giessenbachstr.1, 80748 Garching, Germany

<sup>5</sup> In the following we refer to an event as transient when it has no known quiescent counterpart at any wavelength and to a source which shows a quiescent counterpart in our images or has a catalogued counterpart as variable.

TABLE 1  
FIELDS.

#	RA <sub>2000</sub> <sup>a</sup>	Dec <sub>2000</sub> <sup>a</sup>	Galaxies <sup>b</sup>
A	03:24:36.7	-36:26:21	NGC1326, 1326A, 1326B
B	03:22:41.1	-37:10:54	NGC1316, 1317
C	03:31:04.3	-33:36:42	NGC1350
D	03:36:29.5	-34:52:28	NGC1380, 1380A
E	03:35:44.1	-35:18:50	NGC1373, 1374, 1375, 1379, 1381
F	03:36:49.0	-35:20:55	NGC1379, 1381, 1382, 1387, MCG-06-09-008
G	03:38:34.0	-35:29:58	NGC1399, 1404
H	03:36:45.2	-36:06:17	NGC1369, 1386
I	03:33:37.5	-36:07:19	NGC1365
K	03:42:21.9	-35:16:12	NGC1427, 1428

<sup>a</sup>Coordinates of the centers of the fields.<sup>b</sup>Prominent galaxies within the field of view.

## 2. OBSERVATIONS AND DATA REDUCTION

Observations were obtained with the Wide Field Reimaging CCD Camera (WFCCD) at the 2.5-m Irene du Pont telescope in Las Campanas, Chile. The detector dimensions of 2048×2048 pixels, together with the plate scale of 0".774, provide a circular field of view with ∼12'5 radius. Imaging was performed in the *B*-band as a compromise between avoiding flares from Galactic M-dwarfs (especially bright in the ultra-violet) and increasing the contrast between possible transients and the predominantly early type cluster galaxies (bright in the red part of the spectrum).

For the survey, we selected ten fields covering the 23 brightest Fornax I cluster members (Table 1, Figures available in printed paper). These fields were imaged with a sequence of 120 s exposures repeated up to fifteen times in each of five nights in October and December 2006. Additional single exposures were obtained in five nights in November 2006 (see Table 2 for a complete log). As part of a sequence, a single exposure was taken at each position, after which the telescope slewed to the next field. The resulting distribution of times between consecutive images for each field is given in Figure 1. Throughout the survey a mean intra-day cadence of  $\Delta t = 32.25$  min was achieved. The spread of the observations between October and December 2006 allowed for the possible detection of slowly evolving events with timescales of about one month (e.g., supernovae).

Figure 1 indicates that our primary sensitivity is to variability on ∼32 min timescales. Here, we have a total exposure time of 13.7 days distributed over 616 images (neglecting the once-per-day exposures in November). With a covered area of 0.136 deg<sup>2</sup> per image, this yields a total areal exposure,  $E_A$ , of 1.86 deg<sup>2</sup> days. We have a factor of 5 and 44 larger  $E_A$  for inter-night and inter-month observation intervals, respectively.

Image reduction (bias subtraction, flat fielding) was performed using standard *IRAF* routines<sup>6</sup>. The astrometric solutions were obtained in reference to NOMAD

<sup>6</sup> IRAF was distributed by the National Optical Astronomy Observatories, which are operated by the Association of Universities for Research in Astronomy, Inc., under cooperative agreement with the National Science Foundation

TABLE 2  
OBSERVATION LOG.

Date (UT) <sup>a</sup>	Exposures <sup>b</sup>									
	A	B	C	D	E	F	G	H	I	K
06/10/23	10	10	10	10	9	8	8	8	10	
06/10/24	13	14	13	12	14	10	13	13	13	
06/10/25	lost due to bad weather									
06/11/17	1	1	1	1	1	1	1	1	1	1
06/11/18	1	1	1	1	1	1	1	1	1	1
06/11/19	1	1	1	1	1	1	1	1	1	1
06/11/20	1	1	1	1	1	1	1	1	1	1
06/11/21	1	1	1	1	1	1	1	1	1	1
06/12/19	14	15	14	14	14	14	14	14	14	14
06/12/20	13	13	13	14	13	14	14	14	14	14
06/12/21	12	12	12	12	12	12	12	10	12	12
total <sup>c</sup> :	67	69	67	67	68	64	66	64	66	68

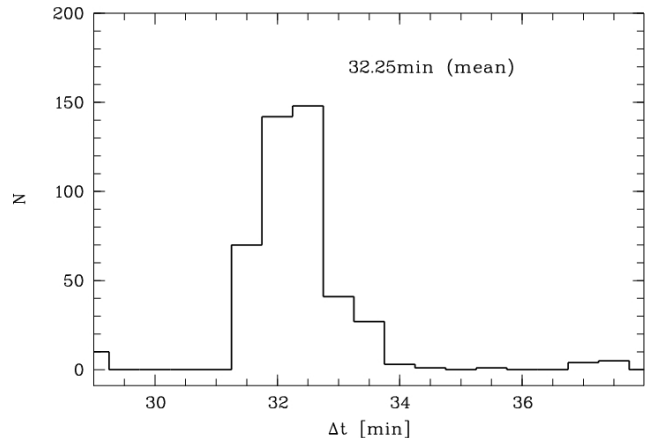
<sup>a</sup>UTC date of observation in the format YY/MM/DD.<sup>b</sup>Number of 120 s *B*-band exposure for each field in a given night.<sup>c</sup>Total number of observations for each field.

FIG. 1.— Time between two consecutive images of a given pointing. The mean cadence is 32.25 min.

(Zacharias et al. 2005) with *ASCfit v3.0*<sup>7</sup>. The strategy to search for transients and variables in single exposures implies that Cosmic-ray removal by median combining of multiple images was not applicable. Hence, we applied a Laplacian algorithm (*lacos.im*; van Dokkum 2001) which allows the identification of Cosmic-rays in single frames.

For absolute photometric calibration we used observations of the standard star field T Phe (Landolt 1992) taken under photometric conditions (2006 November 19). This calibration was applied to the images of the ten Fornax fields obtained during the same night. Exposures from the remaining nights were tied relatively to these absolutely calibrated frames. Here, we selected an ensemble of at least 40 local, non-saturated, non-variable ( $\Delta B < 0.01$  mag) reference stars for each image. The photometric offset between the two observations was estimated by deriving the median brightness offset of these sets of stars with respect to their brightness in the reference frame. This was successively done for all obser-

<sup>7</sup> <http://www.astro.caltech.edu/~pick/ASCFIT/README.ascfit3.html>

vations of a given field, thus providing a common photometric zero-point. The resulting photometric accuracy for point sources is shown in Figure 2. In a typical night a  $5\text{-}\sigma$  limiting magnitude of  $B \sim 22$  mag was reached. Sources brighter than  $B \sim 15$  mag were generally saturated.

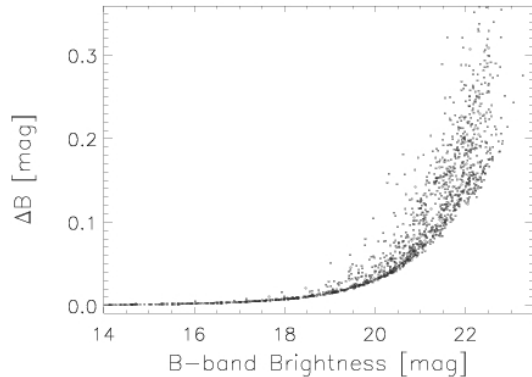


FIG. 2.— Photometric accuracy. Shown are the combined point source measurements of three exposures obtained on 2006 Dec 19 UT. The seeing was  $1''.4$  and a  $5\text{-}\sigma$  limiting magnitude of  $B \sim 22$  mag was reached. Sources brighter than  $B \sim 15$  mag are saturated.

The search for transients and variables was performed in two separate steps. First we applied a point spread function (PSF)-matched image subtraction using a software package based on *ISIS* (Alard 2000). Reference frames for all fields were generated by combining the three best quality exposures taken in November 2006. Candidate transients and variables were detected in the difference images using *SExtractor v2.5.0* (Bertin & Arnouts 1996). For a typical image, this resulted in about 100 sources brighter than  $5\text{-}\sigma$ , out of which all but a few (see below) were subsequently identified by eye as false positives (e.g., image artifacts, Cosmic-ray residuals, PSF distortion, and sources near the rim of the circular field of view which were in the input but not in the reference frame). The PSFs of the resulting candidates were then verified against those of stars in the input images.

The efficiency,  $\epsilon$ , of recovering transients in the difference images was modeled with Monte Carlo simulations. Here, a subset of the survey data was enriched with PSF-matched artificial point sources and subsequently passed through the image subtraction pipeline. The efficiency was then calculated from the ratio of recovered to input test sources. In total we obtained 1.9 Million efficiency points with random location in the field and random magnitudes of  $14 < B < 23$ . As the main driver for our survey was the search for events in nearby galaxies, understanding  $\epsilon$  as function of the local surface brightness became important. Thus, a subset of the efficiency points was placed inside the extend of the bright Fornax cluster members. As expected,  $\epsilon$  was found to decrease with increasing background flux contribution (see Fig. 3a). For “empty” locations ( $B \sim 22.6$  mag  $\text{asec}^{-2}$ ) a recovery efficiency of  $\epsilon = 0.85$  (0.7) was achieved for sources brighter than  $B = 20$  (21.3). In positions with higher surface

brightness ( $B \sim 21.5$ ,  $20.0$  mag  $\text{asec}^{-2}$ ) the maximum efficiency was lower ( $\epsilon = 0.60$ ,  $0.40$ ). Fig 3b shows  $\epsilon$  as function of surface brightness for three test source magnitudes.

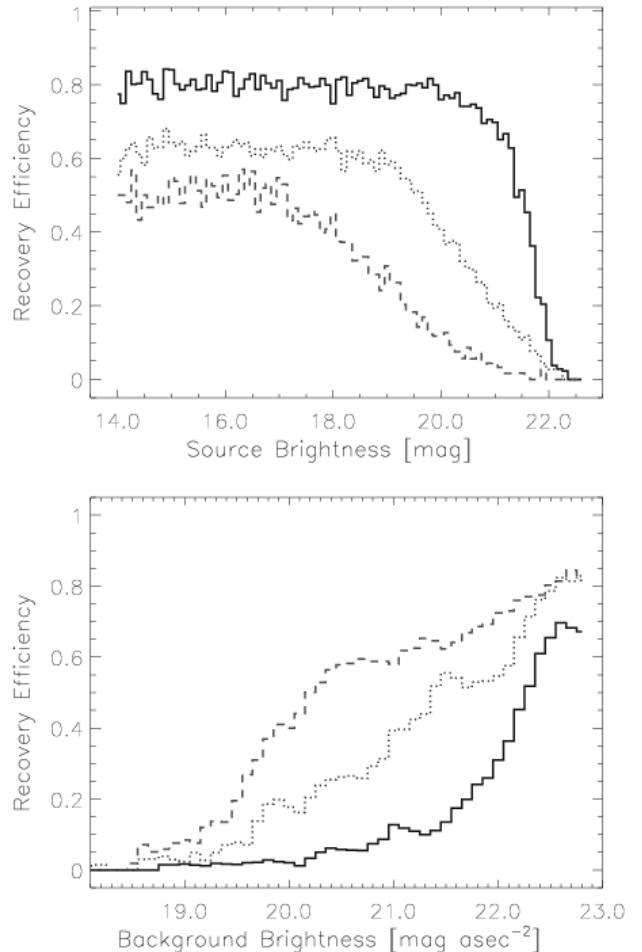


FIG. 3.— left: Transient recovery efficiency as function of source magnitude for three levels of background surface brightness. The solid line ( $B=22.4$  mag  $\text{asec}^{-2}$ ) corresponds to the efficiency away from the Fornax cluster members, while the dotted ( $B=21.5$  mag  $\text{asec}^{-2}$ ) and dashed ( $B=20.0$  mag  $\text{asec}^{-2}$ ) lines are representative for locations within the galaxies. Sources brighter than  $B=15$  are generally saturated. The faint sources cutoff corresponds to the  $5\text{-}\sigma$  detection limits in the difference images. right: Transient recovery efficiency as function of background surface brightness for test sources with  $B=21.3$  (solid),  $19.5$  (dotted) and  $18.0$  (dashed). Fewer efficiency points have been obtained at high surface brightness regions, thus, these bins have the lowest statistic.

In a second step we performed a catalog-based variability search. While this method is inferior to image subtraction for sources overlaying the bright cluster galaxies, it improves the detectivity of low-amplitude, bright variables in the field. For these, image subtraction is typically very sensitive to PSF stability, convolution, and alignment, and residuals unrelated to intrinsic variability may remain. The source catalogs were compiled using *SExtractor v2.5.0* on the photometrically calibrated images (see above). Objects with two or more detections brighter than  $B = 20$  and deviations of more than  $B = 0.1$  mag from their median brightness were selected as candidate variables.

A serious contamination in optical transient and variable searches can come from solar system bodies. However, due to the high ecliptic latitude ( $\beta \approx -53^\circ$ ) observations of the Fornax cluster are only marginally affected. Our choice of using the B-band filter further reduced the impact of asteroids, whose emission peaks at longer wavelength. Moreover repetitive visits of each field throughout the nights were allowing secure astrometric identification of moving objects with proper motions as low as  $3''$  per day. For example, the expected parallax of a Kuiper belt object, at 100 AU from the Sun at that location and time of the year, is  $\sim 33''\text{day}^{-1}$  and  $\sim 3''5\text{day}^{-1}$  due to the Earth and object motion, respectively. Thus, it was not surprising that only one astrometrically variable was found in the survey dataset.

### 3. RESULTS

The search netted seven high-confidence photometric transients and variables. Two, both earlier reported type Ia SNe in NGC 1316, SN 2006dd (Monard 2006) and SN 2006mr (Monard & Folatelli 2006), were only detected in image subtraction. The remaining five objects were variable point sources found with both detection methods. None of them was previously catalogued in SIMBAD<sup>8</sup>, NED<sup>9</sup>, GCVS<sup>10</sup> or detected in the ROSAT/PSPC all-sky survey (Voges et al. 1999). Below we provide a brief description for each of these variable sources (see also Table 3).

#### 3.1. Eruptive variables

Two of the variable sources were detected when they exhibited single flares from their otherwise constant quiescent brightness. The first, FA-1 (Figure 10a), is a faint,  $B = 19.17 \pm 0.03$ , point source that showed a distinct outburst with  $\Delta B = 0.26 \pm 0.04$  mag (Figure 4a). The rise time to peak was shorter than 1 hr ( $2 \times$  cadence) and the decline lasted over  $\sim 2.5$  hrs. The source has a bright near-IR counterpart as detected by 2MASS<sup>11</sup> ( $J = 14.58 \pm 0.03$ ,  $K = 13.65 \pm 0.04$ ). We fitted its  $B - J = 4.59 \pm 0.04$  mag and  $B - K = 5.52 \pm 0.05$  mag colors<sup>12</sup> with stellar templates (Pickles 1998) and found them to be consistent with an M1–2 star. The most likely explanation is a low-amplitude long-decay flare of a UV Ceti type Galactic M1–2 dwarf ( $M_B \sim 11.5$  mag) at a distance of  $\sim 350$  pc.

FH-1 (Figure 10d) was detected when it underwent a strong flare with  $\Delta B = 2.06 \pm 0.15$  mag. It rose to peak in less than 1 hr and decayed to its quiescent brightness of  $B = 20.70 \pm 0.09$  over 1.5 hrs (Figure 4d). FH-1 is bright in the near-IR ( $J = 15.02 \pm 0.02$ ,  $K = 14.29 \pm 0.07$ ) and its colors ( $B - J = 5.68 \pm 0.10$  mag,  $B - K = 6.41 \pm 0.10$  mag) indicate an M3–4 stellar classification. We suggest that this outburst was a long-decay flare of an M3–4 dwarf ( $M_B \sim 12.5$  mag) at a distance of  $\sim 450$  pc.

<sup>8</sup> <http://simbad.u-strasbg.fr/>

<sup>9</sup> <http://nedwww.ipac.caltech.edu/>

<sup>10</sup> [heasarc.gsfc.nasa.gov/W3Browse/all/gcvsnsvars.html](http://heasarc.gsfc.nasa.gov/W3Browse/all/gcvsnsvars.html)

<sup>11</sup> <http://www.ipac.caltech.edu/2mass/>

<sup>12</sup> Here, we assume that the 2MASS observations are representative of the quiescence (or median in case of the non-eruptive sources discussed in § 3.2) brightness. This is supported by generally lower amplitudes in the near-IR compared to the B-band.

#### 3.2. Periodic variables

Regular brightness modulations were shown by three sources. FE-1 (Figure 10c) displayed a nearly sinusoidal variability (Figure 4c) with a maximum amplitude of  $\Delta B = 0.31 \pm 0.05$  mag. A Lomb-Scargle periodogram (Scargle 1982) of the heliocentric corrected lightcurve revealed two possible periods, one at  $0.19025 \pm 0.00002$  days and another at twice this value ( $0.38050 \pm 0.00004$  days; Figure 5). The latter is favored by an apparent difference of  $\Delta B = 0.07 \pm 0.02$  mag in depth of two consecutive minima. Note that FE-1 was included in the overlap of two of our pointings (FE & FF) and thus has twice the data coverage (132 images) compared to the remaining candidates. 2MASS detected the source at  $J = 15.53 \pm 0.05$  and  $K = 15.16 \pm 0.15$ , which, together with a mean brightness of  $B = 16.18 \pm 0.09$ , results in  $B - J = 0.65 \pm 0.10$  mag and  $B - K = 1.02 \pm 0.17$  mag. These colors suggest a spectral type of A7–F0. The source is also included in the GALEX<sup>13</sup> (Martin et al. 2003) source catalog and independent photometry on archival images provides magnitudes  $FUV = 23.4 \pm 0.1$  and  $NUV = 19.04 \pm 0.02$ .

A likely explanation for FE-1 is an eclipsing contact binary system of W Uma type with an orbital period of  $0.38050 \pm 0.00004$  days. This is supported by the apparent two minima in the lightcurve which could indicate the phase of primary and secondary occultation.

The second periodic variable, FK-1 (Figure 10e), was observed as a point source with mean brightness of  $B = 15.42$  and regular non-sinusoidal variations with a period of  $0.31864 \pm 0.00006$  days (Figures 4e,6). The maximum photometric amplitude was  $\Delta B = 0.65 \pm 0.07$  mag. The source has a bright 2MASS counterpart ( $J = 13.42 \pm 0.03$ ,  $K = 12.93 \pm 0.03$ ) and its colors ( $B - J = 2.00 \pm 0.20$  mag,  $B - K = 2.49 \pm 0.20$  mag) resemble those of a G0–9 giant or dwarf.

While the short modulation and lightcurve shape in principle resemble also that of an RRc Lyrae pulsator, the spectral type of G5–9 is inconsistent with this classification. The most likely interpretation for FK-1 is, similar to FE-1, a W Uma type eclipsing binary.

The classification of the remaining variable, FB-1, is more challenging. Its lightcurve displayed apparently erratic variability with an rms of 0.14 mag around the mean brightness of  $B = 18.84 \pm 0.14$  and with a maximum amplitude of  $\Delta B = 0.57 \pm 0.08$  mag (Figure 4b). A Lomb-Scargle periodogram (Figure 7) revealed a number of peaks, the most prominent being at a period of  $0.0585 \pm 0.0001$  days ( $84.24 \pm 0.15$  min). However, the folded lightcurve shows several data points that deviate notably from this phasing. We also note that the power spectrum shows evidence for an additional period of  $\sim 107$  min. Thus, the tentative timescale of modulation has to be taken with caution and confirmation by observations with higher sampling rate will be required.

FB-1 has no 2MASS counterpart to a limiting magnitude of  $J = 17$  which constrains its color to  $B - J < 1.84$  mag. This, together with a GALEX detection at  $NUV = 21.39^{+0.56}_{-0.37}$  and a non-detection in the FUV filter to  $> 21$  mag restricts a stellar classification to A–G. A spectrum obtained with the ESO Multi-

<sup>13</sup> <http://galex.stsci.edu/GR2/?page=mastform>

TABLE 3  
SUMMARY OF DETECTED SOURCES.

#	RA <sub>2000</sub>	Dec <sub>2000</sub>	B <sub>peak</sub> <sup>a</sup> (mag)	B <sub>quiescence</sub> <sup>b</sup> (mag)	Classification	D <sub>proj</sub> <sup>c</sup>
FA-1	03:24:24.56	-36:30:26.5	18.91±0.03	19.17±0.03	M1-2	36 kpc to NGC 1326
FB-1	03:22:31.38	-37:04:01.5	18.48±0.02	18.84±0.14	(?) $\delta$ Scuti/SX Phe	26 kpc to NGC 1317
FE-1	03:36:18.85	-35:14:58.9	16.07±0.01	16.18±0.09	W Uma	29 kpc to NGC 1381
FH-1	03:36:53.67	-36:05:29.9	18.66±0.03	20.70±0.09	M3-4	42 kpc to NGC 1386
FK-1	03:42:33.73	-35:18:29.0	15.20±0.01	15.42±0.20	W Uma	35 kpc to NGC 1427
SN 2006dd	03:22:41.64	-37:12:13.2	17.25±0.03 <sup>d</sup>	-	SN Ia	1.2 kpc to NGC 1316
SN 2006mr	03:22:42.84	-37:12:28.5	16.16±0.03 <sup>e</sup>	-	SN Ia	1.1 kpc to NGC 1316

<sup>a</sup>Observed peak *B*-band magnitude.

<sup>b</sup>Observed mean (for periodic variables) or quiescence (for eruptive variables) *B*-band magnitude.

<sup>c</sup>Projected distance to center of nearest Fornax cluster galaxy.

<sup>d</sup>Observed *B*-band magnitude on 2006 Oct 23.13 UT

<sup>e</sup>Observed *B*-band magnitude on 2006 Nov 17.58 UT

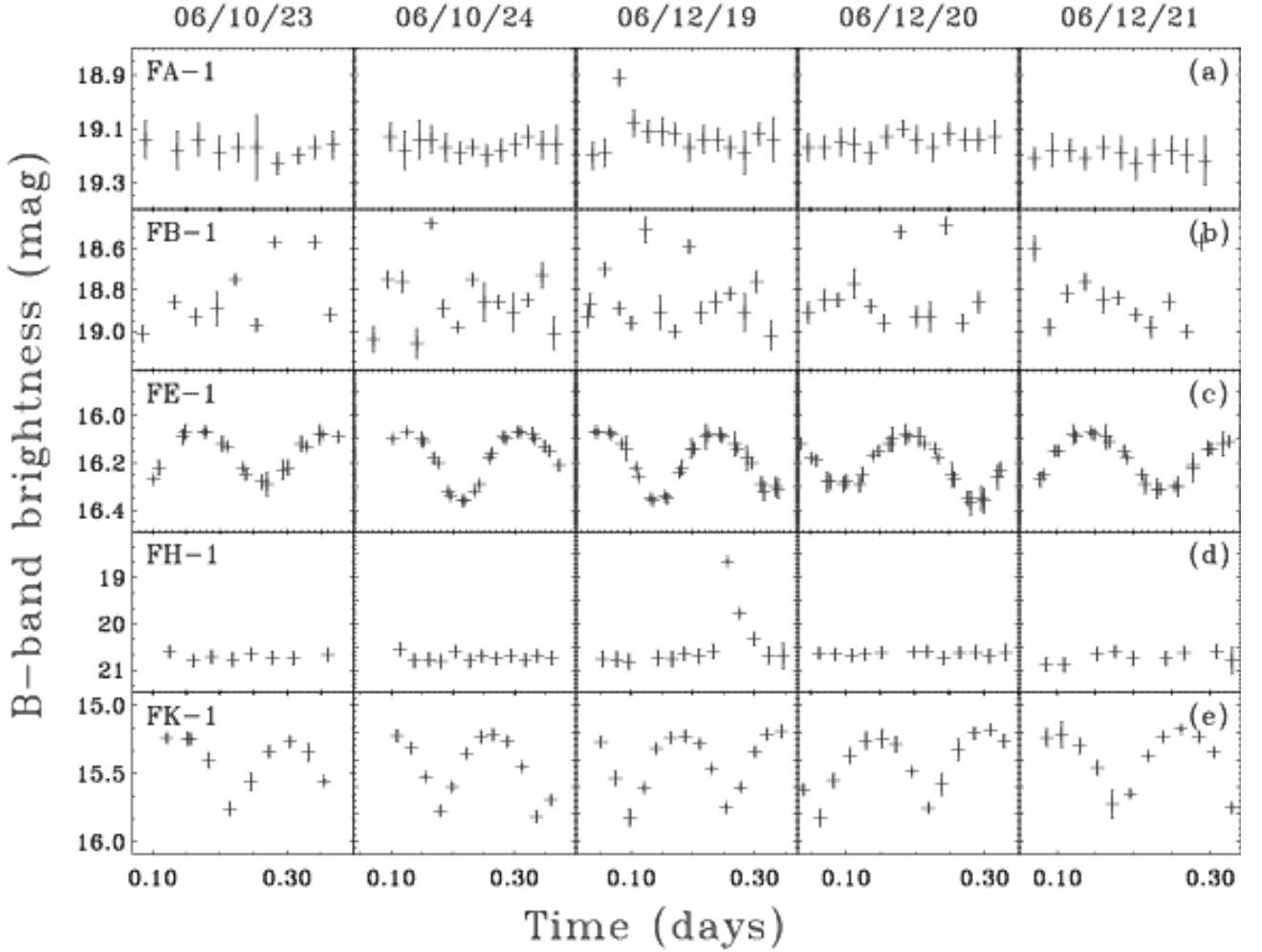


FIG. 4.— Observed *B*-band measurements for the five candidate variables listed in Table 3. Shown are the lightcurves for the five nights with multiple exposures per field (2006 Oct 23, 24 and Dec 19, 20, 21 UTC). Time is given in fractional days (UTC). A compilation of all data is available in electronic form (Table 4).

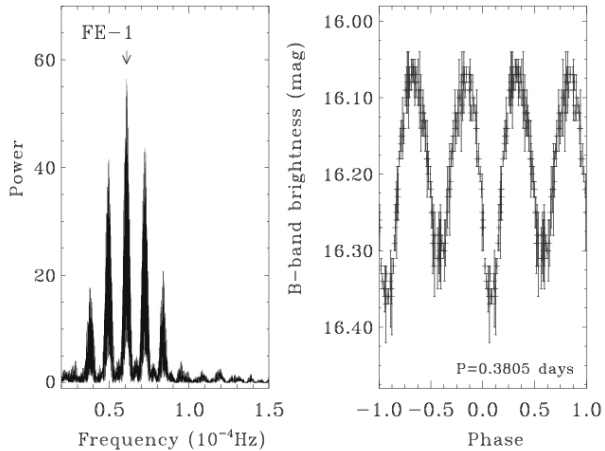


FIG. 5.— Lomb-Scargle periodogram (left) for FE-1 showing that the highest power occurs for at a frequency of  $(6.083 \pm 0.001) \times 10^{-5}$  Hz (or period of  $0.19025 \pm 0.00002$  days). The phase folded heliocentric corrected lightcurve (right) indicates differences in the depth of consecutive minima, suggesting that the real period is likely at twice the above value,  $0.38050 \pm 0.00004$  days.

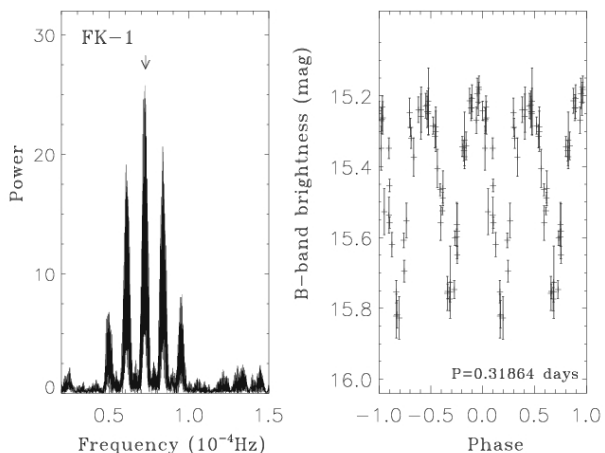


FIG. 6.— Same as Figure 5 for FK-1. The highest power occurs at a frequency of  $(7.264 \pm 0.002) \times 10^{-5}$  Hz (or a period of  $0.15932 \pm 0.00003$  days). The phase folded heliocentric corrected lightcurve again indicates differences in the depth of consecutive minima, suggesting that the real period is likely  $0.31864 \pm 0.00006$  days.

Mode Instrument (EMMI) at the NTT, La Silla, shows a blue continuum with prominent Balmer absorption lines (Figure 8). A comparison with template stellar spectra (Pickles 1998) suggests an A7 classification. This spectral range is populated by pulsators such as  $\delta$  Scuti stars and RR Lyrae. Of those, only  $\delta$  Scuti stars, and the phenomenologically<sup>14</sup> similar SX Phe stars (Rodríguez et al. 1990), exhibit modulations on timescales as short as detected for FB-1. As indicated by the number of short period peaks in the periodogram, we may have to consider also events with periods below 84 mins. Some white dwarf systems do show periodic pul-

<sup>14</sup>  $\delta$  Scuti and SX Phe stars are generally distinguished by their hosting stellar population and metallicity. This can not be accomplished with the available data.

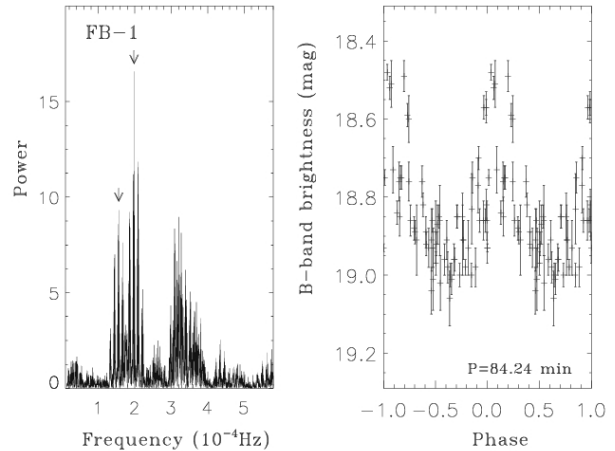


FIG. 7.— Same as Figure 5 for FB-1. The periodogram shows a large number of peaks, with the most prominent at  $(1.975 \pm 0.005) \times 10^{-4}$  Hz (84.24  $\pm$  0.15 min). A second period occurs at 107 min.

sations below 30 min. ZZ Ceti type sources have white dwarf temperatures (11–12 kK; Bergeron et al. 2004) in agreement with the observed colors (Kawka et al. 2006). However, the lack of pressure broadening of the Balmer absorption lines rules out the white dwarf scenario. Awaiting further test of the periodic modulation, we find that a Galactic  $\delta$  Scuti or SX Phe star appears to be the most intriguing interpretation for FB-1.

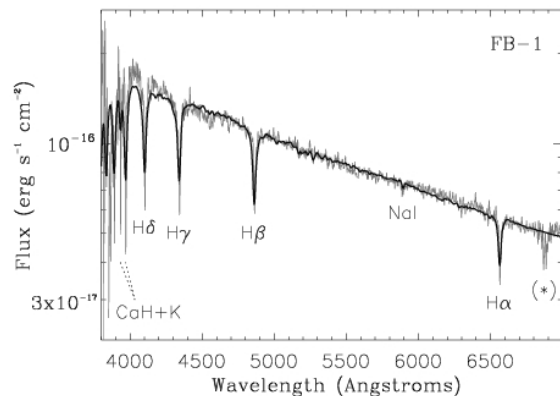


FIG. 8.— NTT/EMMI spectrum (grey) of FB-1 obtained on 2007 Dec 12.19 UT using the low-dispersion mode (RILD) with grism#5 (instrumental FWHM=4.5 Å). The data were reduced with customized IRAF routines and flux calibrated in comparison to the spectro-photometric standard star LTT377 (Hamuy et al. 1992). The black solid line shows an A7V template spectrum from Pickles (1998). Prominent spectral features are indicated.

#### 4. DISCUSSION

Here were reported the results of a dedicated search for optical fast transients and variables in the environment of the Fornax I galaxy cluster. In total, the survey netted two transients and five high-amplitude ( $\Delta B > 0.1$  mag) variable sources. Both transients have been detected as a result of the inter-month sampling

of our observations and have independently been reported and classified as type Ia supernovae in NGC 1216 (Monard 2006; Monard & Folatelli 2006). The properties of the five variables suggests that they are located in the foreground to the Fornax I cluster and belong to the Milky Way stellar population. This is in agreement with the large projected distance (26–42 kpc) of the events to the nearest Fornax galaxies (see Table 3). Two of the variables were identified as flares from M-dwarfs, while other two are likely eclipsing binaries of the W Uma type. The remaining variable shows indications for a very short periodicity ( $\sim 84$  min), and spectroscopy suggests it to be a  $\delta$  Scuti or SX Phe star. No genuine fast transient brighter than  $B = 21.3$  has been detected.

Surveys, like the one presented here, can offer valuable guidance for the planning and execution of the next generation of transient experiments. In order to provide relevant event rates, a complete identification of all sources detected with a given choice of cadence, filter, depth, amplitude, and field selection, is required. This will pose inevitable challenges for follow-up limited projects like Pan-STARRS and LSST. However, at least for variables, multi-band photometry and good temporal coverage can already be strong indicators for the nature of an event, as demonstrated for the Fornax sources. Indeed, automatic cross-matching with UV to near-IR source catalogs with a similar depth as the surveys will be vital for the success of the future large optical projects.

#### 4.1. All-Sky Rate of Fast Transients

In the following, we will discuss the estimates and expectations for transients on timescales of  $\sim 32$  min and with apparent peak brightness of  $15 < B < 21.3$ . We start by determining the upper limit on the rate of cosmological fast transients not associated with any of the Fornax cluster galaxies. As described in § 2, the areal survey exposure is  $E_A = 1.86 \text{ deg}^2$  and the efficiency for a single detection of a field source brighter than  $B = 21.3$  is  $\epsilon = 0.7$ . As we require a candidate to be found in at least two images,  $\epsilon$  needs to be squared. The non-detection of fast transients in the survey translates into a 95 % Poisson upper limit of  $N=3$  events (Gehrels 1986). The corresponding rate follows from

$$r_A = \frac{N}{\epsilon^2 \cdot E_A} \quad (1)$$

as  $r_A < 3.3 \text{ events day}^{-1} \text{ deg}^{-2}$ , or an annual all-sky rate of  $r_A < 5 \times 10^7$ . Note, that these limits are valid only for an event population that is homogeneously distributed over the sky. In other words, the detection probability has to be independent of the field selection. Under this assumption, we can match our estimates with previously obtained results, e.g., from the Deep Lens Survey transient search (DLS; Becker et al. 2004). Indeed, the Fornax survey is very similar to the DLS with respect to exposure (1.38 vs 1.1  $\text{deg}^2 \text{ days}$ ) and probed timescale (32 vs 22 min). As also no genuine fast transient was found in the DLS, the the event rate is comparable.

#### 4.2. Rates of Fast Transients in Nearby Galaxies

The main motivation of our survey was the exploration of the transient and variable population in a specific environment, namely in a galaxy cluster with known distance and known stellar mass. For this purpose, we will

now calculate the specific rate of fast transients per unit stellar mass, or its proxy, the  $B$ -band luminosity.

As discussed above (see also Fig. 3),  $\epsilon$  is not only a function of the magnitude of a transient,  $M_T$ , but depends also on the underlying surface brightness,  $m_{\text{SB}}$ . Similarly, the product of the luminosity,  $L_{\text{SB},i}$ , enclosed in a surface brightness bin,  $m_{\text{SB},i}$ , and the relative exposure,  $t$ , is different for all targeted Fornax galaxies. Here,  $t$  denotes the time a given galaxy was probed for transients on timescales of the 32 min cadence. We start by calculating  $L_{\text{SB},i}$  for each galaxy listed in Table 1, with  $i$  running from the saturation limit of 16.7 mag  $\text{asec}^{-2}$  to the sky background brightness of 22.6 mag  $\text{asec}^{-2}$  in steps of 0.1 mag. Next, we estimate the survey exposure,  $E_{\text{SB},i}$ , for each  $m_{\text{SB},i}$  in units<sup>15</sup> of  $M_{B,\odot}$  years by summing  $L_{\text{SB},i} \cdot t$  for all galaxies. The rate of transients as function of the brightness can then be calculated as

$$r(M_T) = \sum_i \frac{N(M_T)}{\epsilon(M_T, m_{\text{SB}})_i^2 \cdot E_{\text{SB},i}} \quad (2)$$

Formerly, the number of detected transients,  $N$ , also depends on the peak brightness. However, here we use again the 95 % Poisson upper limit of  $N(M_T) = N = 3$  events, as no event in the entire probed range of  $15 < B < 21.3$  was detected.

The result is presented in Figure 9, where we show the upper limit on the rate as function of transient magnitude. As expected, the brightest events ( $m_B < 18.5$ ,  $M_B < -12.4$ ) have the lowest limits ( $r < 10^{-8}$  events  $M_{B,\odot}^{-1} \text{ yr}^{-1}$ ). For the Milky Way disk ( $M_B = -19.9$ ; Quillen & Sarajedini 1997) this translates into  $< 140$  events per year, e.g., a few times more than the classical novae rate. One could argue that any Galactic transient population brighter than classical novae and with a comparable frequency may have been discovered already. However, the short timescales tested in our survey require a significantly higher cadence than typically used in transient searches. Fast transients may have previously been detected in single images, but simply discarded as unconfirmed or spurious events. However, there have been a number of planetary transit and variable star studies, which offer the required high cadence (e.g.; Kane et al. 2005; Kraus et al. 2007; Lister et al. 2007). These experiments typically target dense Galactic fields and thus a large stellar population. Unfortunately, results on transients, as opposed to transits, are rarely recorded or published.

## 5. CONCLUSION

The existence of fast transients requires further constraint with specialized experiments. The most exciting facility in this respect will be the Palomar Transient Factory (PTF, Rau et al., in prep.), a dedicated transient survey instrument at the Palomar 48-inch telescope with expected first light in Winter 2008. The PTF will use a 7.8 square degree field of view to perform a number of transient searches on various time scales. The large field of view will allow us to cover galaxy clusters with fewer pointings, thus increasing the total stellar mass observed at a given cadence.

<sup>15</sup> Here, we use an absolute solar  $B$ -band magnitude of  $M_{B,\odot} = 5.48$

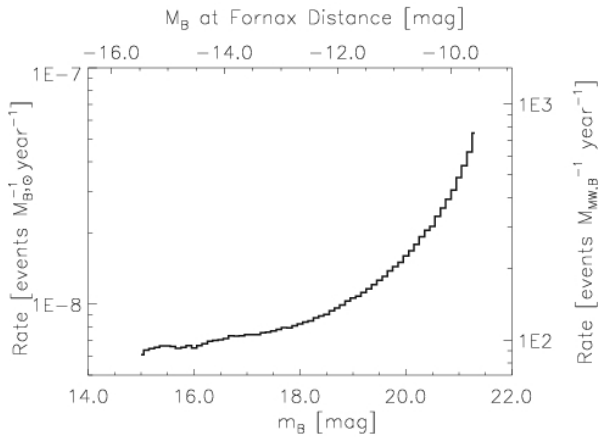


FIG. 9.— 95% Poisson upper limit on the rate of transients on timescales of 32 min as function of peak brightness.

However, we have shown that the probability of detecting a transient strongly depends on the local surface brightness. While this is not a surprising result, its relevance for future searches in nearby galaxies needs to be understood. There will always be the need for a compromise between limiting magnitude of an event to be detected and galaxy fraction covered. Larger apertures or longer exposures are not necessarily improving the detection probability for faint events. Although more source

photons will be collected, also more host light is received and a larger extend of the galaxy will be above saturation. The main factor for success will be the image quality. At a given surface brightness, a narrower PSF will increase the signal-to-noise, and thus, the probability for a detection.

We are grateful to Paul Price for providing his image subtraction code and to Carol Wainwright for his contribution to the pipeline. We thank Mara Salvato, Mansi M. Kasliwal and S. Bradley Cenko for discussion and constructive criticism. We thank the referee for his stimulating comments and suggestions. This work is based on in part on observations collected at the European Southern Observatory, Chile. This publication makes use of data products from the Two Micron All Sky Survey, which is a joint project of the University of Massachusetts and the Infrared Processing and Analysis Center/California Institute of Technology, funded by the National Aeronautics and Space Administration and the National Science Foundation. This research has made use of the NASA/IPCA Extragalactic Database (NED) which is operated by the Jet Propulsion Laboratory, California Institute of Technology, under contract with the National Aeronautics and Space Administration. This work is supported in part by grants from the National Science Foundation and NASA.

#### REFERENCES

- Alard, C. 2000, *A&AS*, 144, 363  
 Becker, A. C., Wittman, D. M., Boeshaar, P. C., et al. 2004, *ApJ*, 611, 418  
 Bergeron, P., Fontaine, G., Billères, M., et al. 2004, *ApJ*, 600, 404  
 Bertin, E. & Arnouts, S. 1996, *A&AS*, 117, 393  
 Gehrels, N. 1986, *ApJ*, 303, 336  
 Grillmair, C. J., Forbes, D. A., Brodie, J. P., et al. 1999, *AJ*, 117, 167  
 Hamuy, M., Walker, A. R., Suntzeff, N. B., et al. 1992, *PASP*, 104, 533  
 Kaiser, N., Aussel, H., Burke, B. E., et al. 2002, in Presented at the Society of Photo-Optical Instrumentation Engineers (SPIE) Conference, Vol. 4836, Survey and Other Telescope Technologies and Discoveries. Edited by Tyson, J. Anthony; Wolff, Sidney. Proceedings of the SPIE, Volume 4836, pp. 154-164 (2002)., ed. J. A. Tyson & S. Wolff, 154  
 Kane, S. R., Lister, T. A., Cameron, A. C., et al. 2005, *MNRAS*, 362, 117  
 Kasliwal, M. M., Cenko, S. B., Kulkarni, S. R., et al. 2007, *ArXiv e-prints*, 0708.0226  
 Kawka, A., Vennes, S., Oswalt, T. D., et al. 2006, *ApJ*, 643, L123  
 Klotz, A., Boer, M., & Atteia, J. 2007, *GRB Coordinates Network*, 6769, 1  
 Kraus, A. L., Craine, E. R., Giampapa, M. S., et al. 2007, *AJ*, 134, 1488  
 Kulkarni, S. R., Ofek, E. O., Rau, A., et al. 2007, *Nature*, 447, 458  
 Kulkarni, S. R. & Rau, A. 2006, *ApJ*, 644, L63  
 Landolt, A. U. 1992, *AJ*, 104, 340  
 Lister, T. A., West, R. G., Wilson, D. M., et al. 2007, *MNRAS*, 379, 647  
 Martin, C., Barlow, T., Barnhart, W., et al. 2003, in Presented at the Society of Photo-Optical Instrumentation Engineers (SPIE) Conference, Vol. 4854, Future EUV/UV and Visible Space Astrophysics Missions and Instrumentation. Edited by J. Chris Blades, Oswald H. W. Siegmund. Proceedings of the SPIE, Volume 4854, pp. 336-350 (2003)., ed. J. C. Blades & O. H. W. Siegmund, 336  
 Monard, L. A. G. 2006, *Central Bureau Electronic Telegrams*, 553, 1  
 Monard, L. A. G. & Folatelli, G. 2006, *Central Bureau Electronic Telegrams*, 723, 1  
 Morales-Rueda, L., Groot, P. J., Augusteijn, T., et al. 2006, *MNRAS*, 371, 1681  
 Ofek, E. O., Cameron, P. B., Kasliwal, M. M., et al. 2007a, *ApJ*, 659, L13  
 Ofek, E. O., Kulkarni, S. R., Rau, A., et al. 2007b, *ArXiv e-prints*, 710  
 Pagani, C., Barthelmy, S. D., Cummings, J. R., et al. 2007, *GRB Coordinates Network*, 6489, 1  
 Pastorello, A., Smartt, S. J., Mattila, S., et al. 2007, *Nature*, 447, 829  
 Pickles, A. J. 1998, *PASP*, 110, 863  
 Quillen, A. C., & Sarajedini, V. L., 1997, *AJ*, 115, 1412  
 Quimby, R. M., Aldering, G., Wheeler, J. C., et al. 2007, *ApJ*, 668, L99  
 Ramsay, G., Napiwotzki, R., Hakala, P., et al. 2006, *MNRAS*, 371, 957  
 Rau, A., Kulkarni, S. R., Ofek, E. O., et al. 2007, *ApJ*, 659, 1536  
 Rodriguez, E., Rolland, A., & Lopez de Coca, P. 1990, *Ap&SS*, 169, 113  
 Rykoff, E. S., Aharonian, F., Akerlof, C. W., et al. 2005, *ApJ*, 631, 1032  
 Scargle, J. D. 1982, *ApJ*, 263, 835  
 Schlegel, D. J., Finkbeiner, D. P., Davis, M., 1998, *ApJ*, 500, 525  
 Schmidt, B. P., Keller, S. C., Francis, P. J., et al. 2005, in *Bulletin of the American Astronomical Society*, Vol. 37, *Bulletin of the American Astronomical Society*, 457  
 Smith, N., Li, W., Foley, R. J., et al. 2007, *ApJ*, 666, 1116  
 Stefanescu, A., Slowikowska, A., Kanbach, G., et al. 2007, *GRB Coordinates Network*, 6508, 1  
 Tyson, A. 2005, in *Astronomical Society of the Pacific Conference Series*, Vol. 339, *Observing Dark Energy*, ed. S. C. Wolff & T. R. Lauer, 95  
 van Dokkum, P. G. 2001, *PASP*, 113, 1420  
 Voges, W., Aschenbach, B., Boller, T., et al. 1999, *A&A*, 349, 389  
 Zacharias, N., Monet, D. G., Levine, S. E., et al. 2005, *VizieR Online Data Catalog*, 1297, 0



MJD	B-band Mag	Err
51	19.09	0.13
50	19.13	0.13
49	19.17	0.13
48	19.20	0.13
47	19.23	0.13
46	19.26	0.13
45	19.29	0.13
44	19.32	0.13
43	19.35	0.13
42	19.38	0.13
41	19.41	0.13
40	19.44	0.13
39	19.47	0.13
38	19.50	0.13
37	19.53	0.13
36	19.56	0.13
35	19.59	0.13
34	19.62	0.13
33	19.65	0.13
32	19.68	0.13
31	19.71	0.13
30	19.74	0.13
29	19.77	0.13
28	19.80	0.13
27	19.83	0.13
26	19.86	0.13
25	19.89	0.13
24	19.92	0.13
23	19.95	0.13
22	19.98	0.13
21	20.01	0.13
20	20.04	0.13
19	20.07	0.13
18	20.10	0.13
17	20.13	0.13
16	20.16	0.13
15	20.19	0.13
14	20.22	0.13
13	20.25	0.13
12	20.28	0.13
11	20.31	0.13
10	20.34	0.13
9	20.37	0.13
8	20.40	0.13
7	20.43	0.13
6	20.46	0.13
5	20.49	0.13
4	20.52	0.13
3	20.55	0.13
2	20.58	0.13
1	20.61	0.13
0	20.64	0.13
51	19.09	0.13
50	19.13	0.13
49	19.17	0.13
48	19.20	0.13
47	19.23	0.13
46	19.26	0.13
45	19.29	0.13
44	19.32	0.13
43	19.35	0.13
42	19.38	0.13
41	19.41	0.13
40	19.44	0.13
39	19.47	0.13
38	19.50	0.13
37	19.53	0.13
36	19.56	0.13
35	19.59	0.13
34	19.62	0.13
33	19.65	0.13
32	19.68	0.13
31	19.71	0.13
30	19.74	0.13
29	19.77	0.13
28	19.80	0.13
27	19.83	0.13
26	19.86	0.13
25	19.89	0.13
24	19.92	0.13
23	19.95	0.13
22	19.98	0.13
21	20.01	0.13
20	20.04	0.13
19	20.07	0.13
18	20.10	0.13
17	20.13	0.13
16	20.16	0.13
15	20.19	0.13
14	20.22	0.13
13	20.25	0.13
12	20.28	0.13
11	20.31	0.13
10	20.34	0.13
9	20.37	0.13
8	20.40	0.13
7	20.43	0.13
6	20.46	0.13
5	20.49	0.13
4	20.52	0.13
3	20.55	0.13
2	20.58	0.13
1	20.61	0.13
0	20.64	0.13

FA-1

FB-1



MJD	B-band Mag	Err
54400.237783	16.25	0.02
54400.267773	16.29	0.02
54400.298886	16.32	0.03
54400.326336	16.13	0.01
54400.352533	16.08	0.01
54400.374944	16.11	0.01
54400.396433	16.20	0.01
54400.418644	16.34	0.01
54400.440855	16.36	0.01
54400.462666	16.38	0.02
54400.484877	16.18	0.01
54400.507088	16.10	0.01
54400.529299	16.07	0.01
54400.551510	16.28	0.02
54400.573721	16.28	0.01
54400.595932	16.17	0.02
54400.618143	16.07	0.01
54400.640354	16.17	0.01
54400.662565	16.08	0.01
54400.684776	16.32	0.01
54400.706987	16.33	0.03
54400.729198	16.33	0.03
54400.751409	16.33	0.03
54400.773620	16.17	0.01
54400.795831	16.08	0.01
54400.818042	16.09	0.01
54400.840253	16.24	0.02
54400.862464	16.20	0.02
54400.884675	16.32	0.04
54400.906886	16.31	0.02
54400.929097	16.12	0.01
54400.951308	16.32	0.03
54400.973519	16.22	0.03
54400.995730	16.33	0.03
54401.017941	16.33	0.03
54401.040152	16.33	0.03
54401.062363	16.33	0.03
54401.084574	16.33	0.03
54401.106785	16.33	0.03
54401.128996	16.33	0.03
54401.151207	16.33	0.03
54401.173418	16.33	0.03
54401.195629	16.33	0.03
54401.217840	16.33	0.03
54401.240051	16.33	0.03
54401.262262	16.33	0.03
54401.284473	16.33	0.03
54401.306684	16.33	0.03
54401.328895	16.33	0.03
54401.351106	16.33	0.03
54401.373317	16.33	0.03
54401.395528	16.33	0.03
54401.417739	16.33	0.03
54401.439950	16.33	0.03
54401.462161	16.33	0.03
54401.484372	16.33	0.03
54401.506583	16.33	0.03
54401.528794	16.33	0.03
54401.551005	16.33	0.03
54401.573216	16.33	0.03
54401.595427	16.33	0.03
54401.617638	16.33	0.03
54401.639849	16.33	0.03
54401.662060	16.33	0.03
54401.684271	16.33	0.03
54401.706482	16.33	0.03
54401.728693	16.33	0.03
54401.750904	16.33	0.03
54401.773115	16.33	0.03
54401.795326	16.33	0.03
54401.817537	16.33	0.03
54401.839748	16.33	0.03
54401.861959	16.33	0.03
54401.884170	16.33	0.03
54401.906381	16.33	0.03
54401.928592	16.33	0.03
54401.950803	16.33	0.03
54401.973014	16.33	0.03
54401.995225	16.33	0.03
54402.017436	16.33	0.03
54402.039647	16.33	0.03
54402.061858	16.33	0.03
54402.084069	16.33	0.03
54402.106280	16.33	0.03
54402.128491	16.33	0.03
54402.150702	16.33	0.03
54402.172913	16.33	0.03
54402.195124	16.33	0.03
54402.217335	16.33	0.03
54402.239546	16.33	0.03
54402.261757	16.33	0.03
54402.283968	16.33	0.03
54402.306179	16.33	0.03
54402.328390	16.33	0.03
54402.350601	16.33	0.03
54402.372812	16.33	0.03
54402.395023	16.33	0.03
54402.417234	16.33	0.03
54402.439445	16.33	0.03
54402.461656	16.33	0.03
54402.483867	16.33	0.03
54402.506078	16.33	0.03
54402.528289	16.33	0.03
54402.550500	16.33	0.03
54402.572711	16.33	0.03
54402.594922	16.33	0.03
54402.617133	16.33	0.03
54402.639344	16.33	0.03
54402.661555	16.33	0.03
54402.683766	16.33	0.03
54402.705977	16.33	0.03
54402.728188	16.33	0.03
54402.750399	16.33	0.03
54402.772610	16.33	0.03
54402.794821	16.33	0.03
54402.817032	16.33	0.03
54402.839243	16.33	0.03
54402.861454	16.33	0.03
54402.883665	16.33	0.03
54402.905876	16.33	0.03
54402.928087	16.33	0.03
54402.950298	16.33	0.03
54402.972509	16.33	0.03
54402.994720	16.33	0.03
54403.016931	16.33	0.03
54403.039142	16.33	0.03
54403.061353	16.33	0.03
54403.083564	16.33	0.03
54403.105775	16.33	0.03
54403.127986	16.33	0.03
54403.150197	16.33	0.03
54403.172408	16.33	0.03
54403.194619	16.33	0.03
54403.216830	16.33	0.03
54403.239041	16.33	0.03
54403.261252	16.33	0.03
54403.283463	16.33	0.03
54403.305674	16.33	0.03
54403.327885	16.33	0.03
54403.350096	16.33	0.03
54403.372307	16.33	0.03
54403.394518	16.33	0.03
54403.416729	16.33	0.03
54403.438940	16.33	0.03
54403.461151	16.33	0.03
54403.483362	16.33	0.03
54403.505573	16.33	0.03
54403.527784	16.33	0.03
54403.550095	16.33	0.03
54403.572306	16.33	0.03
54403.594517	16.33	0.03
54403.616728	16.33	0.03
54403.638939	16.33	0.03
54403.661150	16.33	0.03
54403.683361	16.33	0.03
54403.705572	16.33	0.03
54403.727783	16.33	0.03
54403.750094	16.33	0.03
54403.772305	16.33	0.03
54403.794516	16.33	0.03
54403.816727	16.33	0.03
54403.838938	16.33	0.03
54403.861149	16.33	0.03
54403.883360	16.33	0.03
54403.905571	16.33	0.03
54403.927782	16.33	0.03
54403.950093	16.33	0.03
54403.972304	16.33	0.03
54403.994515	16.33	0.03

FH-1

54403.994515	20.60	0.11
54404.016726	20.60	0.11
54404.038937	20.60	0.11
54404.061148	20.60	0.11
54404.083359	20.60	0.11
54404.105570	20.60	0.11
54404.127781	20.60	0.11
54404.150092	20.60	0.11
54404.172303	20.60	0.11
54404.194514	20.60	0.11
54404.216725	20.60	0.11
54404.238936	20.60	0.11
54404.261147	20.60	0.11
54404.283358	20.60	0.11
54404.305569	20.60	0.11
54404.327780	20.60	0.11
54404.350091	20.60	0.11
54404.372302	20.60	0.11
54404.394513	20.60	0.11
54404.416724	20.60	0.11
54404.438935	20.60	0.11
54404.461146	20.60	0.11
54404.483357	20.60	0.11
54404.505568	20.60	0.11
54404.527779	20.60	0.11
54404.550090	20.60	0.11
54404.572301	20.60	0.11
54404.594512	20.60	0.11
54404.616723	20.60	0.11
54404.638934	20.60	0.11
54404.661145	20.60	0.11
54404.683356	20.60	0.11
54404.705567	20.60	0.11
54404.727778	20.60	0.11
54404.750089	20.60	0.11
54404.772300	20.60	0.11
54404.794511	20.60	0.11
54404.816722	20.60	0.11
54404.838933	20.60	0.11
54404.861144	20.60	0.11
54404.883355	20.60	0.11
54404.905566	20.60	0.11
54404.927777	20.60	0.11
54404.950088	20.60	0.11
54404.972309	20.60	0.11
54404.994520	20.60	0.11

MJD	B-band Mag	Err
54089.33192	20.62	0.17
54090.08737	20.88	0.14
54090.10922	20.89	0.14
54090.15416	20.66	0.13
54090.17598	20.60	0.11
54090.19805	20.75	0.14
54090.24210	20.75	0.14
54090.26142	20.63	0.14
54090.30681	20.60	0.14
54090.32935	20.80	0.28
FK-1		
54031.12012	19.24	0.02
54031.15399	19.24	0.04
54031.15669	19.25	0.03
54031.18529	19.40	0.05
54031.21552	19.75	0.04
54031.24486	19.56	0.06
54031.27346	19.34	0.03
54031.30480	19.36	0.03
54031.33144	19.34	0.06
54031.35309	19.33	0.01
54031.38335	19.33	0.03
54031.41338	19.32	0.01
54031.44368	19.32	0.03
54031.47366	19.33	0.02
54031.50333	19.33	0.02
54031.53277	19.33	0.02
54031.56227	19.33	0.02
54031.59187	19.23	0.03
54031.62133	19.21	0.03
54031.65034	19.26	0.03
54031.67936	19.45	0.01
54031.70845	19.81	0.03
54031.73728	19.69	0.03
54031.76553	19.54	0.04
54031.79333	19.35	0.02
54031.82133	19.23	0.04
54031.84971	19.23	0.03
54031.87798	19.24	0.03
54031.90641	19.23	0.06
54031.93490	19.23	0.02
54031.96274	19.33	0.03
54031.99090	19.33	0.02
54032.01921	19.33	0.03
54032.04790	19.33	0.03
54032.07633	19.33	0.03
54032.10407	19.32	0.03
54032.13227	19.32	0.03
54032.16070	19.32	0.03
54032.18927	19.38	0.01
54032.21772	19.46	0.02
54032.24550	19.56	0.02
54032.27391	19.34	0.03
54032.30189	19.31	0.03
54032.32933	19.33	0.04
54032.35633	19.33	0.03
54032.38369	19.32	0.06
54032.41033	19.32	0.04
54032.43743	19.32	0.05
54032.46433	19.32	0.06
54032.49193	19.24	0.06
54032.51940	19.28	0.05
54032.54722	19.48	0.01
54032.57462	19.75	0.02
54032.60161	19.35	0.02
54032.62890	19.35	0.02
54032.65610	19.35	0.03
54032.68391	19.35	0.03
54032.71140	19.35	0.04
54032.73871	19.35	0.06
54032.76601	19.31	0.09
54032.79336	19.30	0.05
54032.82000	19.46	0.04
54032.84781	19.72	0.10
54032.87578	19.64	0.02
54032.90396	19.37	0.03
54032.93194	19.23	0.03
54032.95983	19.17	0.01
54032.98724	19.23	0.03
54033.01454	19.34	0.03
54033.04177	19.34	0.03
54033.06907	19.75	0.03

TABLE 4 DATA TABLE FOR VARIABLES FOUND IN THE SURVEY. (FOR ELECTRONIC VERSION)

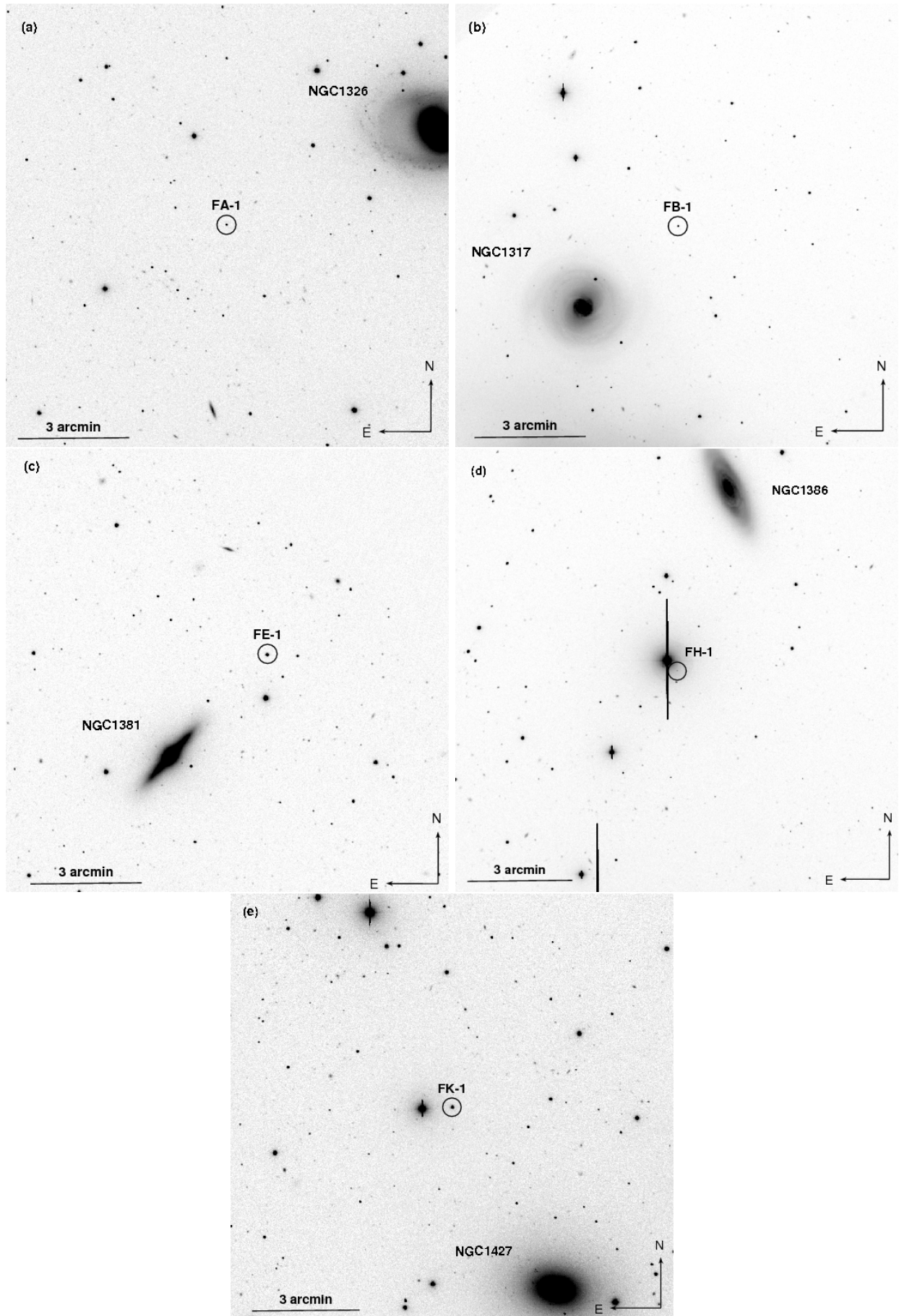


FIG. 10.— Finding charts.